AIAA JOURNAL
Vol. 39, No. 6, June 2001

Sensitivity Analysis of Unsteady Inviscid Flow Through Turbomachinery Cascades

Razvan Florea* and Kenneth C. Hall†
Duke University, Durham, North Carolina 27708-0300

We present a novel sensitivity analysis for predicting the effect of airfoil shape on the unsteady aerodynamic and aeroacoustic response of turbomachinery blading. The nominal steady and unsteady flow in a cascade of turbomachinery blades is modeled using the steady Euler equations and the time-linearized Euler equations, respectively. Both the steady and unsteady Euler equations are solved using a two-step finite-volume Lax–Wendroff discretization with multigrid acceleration. We compute the unsteady aerodynamic loads due to both incoming gusts and plunging motion of the cascade airfoils. Once the nominal steady and unsteady flows have been computed, a sensitivity analysis is performed using the discrete adjoint equations of the computational fluid dynamics scheme used to discretize the Euler equations. For each objective function (e.g., the amplitude peak of the aeroelastic blade motion), the resulting adjoint equations are solved using the adjoint Lax–Wendroff scheme, which is also accelerated using a multigrid technique. Once the adjoint equations have been solved, the computed adjoint variables may be used to compute rapidly the sensitivities of the aeroelastic and aeroacoustic objective functions due to arbitrary changes in geometry. The method is computationally efficient, with similar convergence rate histories for both the nominal and the adjoint solutions. To demonstrate the utility of the present method, we use the sensitivity analysis to redesign the shape of the airfoils of a cascade for increased aeroelastic stability. We also redesign the shape of the airfoils of an exit guide vane for reduced downstream radiated noise.

I. Introduction

AEROELASTICITY and aeroacoustics play important roles in the design of modern turbomachinery blading. For example, turbomachinery blades are subjected to unsteady aerodynamics forces that cause them to vibrate. This vibration can, if large enough, result in high cycle fatigue (HCF), causing the airfoils to break, severely damaging or destroying the engine. Hence, after the steady aerodynamic design phase, detailed but computationally expensive aeroelastic studies are performed to determine whether the blades will be aeroelastically stable and have acceptable fatigue life. If the blade fails to meet these aeromechanical requirements, it is redesigned, and the process is repeated, increasing the time and cost required to design the engine. Similarly, studies are performed to predict the radiated noise from the aircraft engine. For a given blade row, sources of aeroacoustic excitation include inlet distortions and viscous wakes from upstream blade rows. Examples of techniques to reduce the radiated noise are proper selection of blade numbers, larger axial distance between blade rows, and installation of acoustical liners. In a recent study, Gliebe[1] indicates that new modern design trends for a high bypass ratio engine require more source noise control by design to maintain even current engine noise levels, let alone reduce noise levels significantly below those of current engines. One needs not only the capability to predict aeroelastic and aeroacoustic behavior of the airfoils in a turbomachine, but also the capability to understand the influence of design changes.

In the present analysis, we use the time-linearized (frequency domain) approach to predict the unsteady flow about cascades due to incoming disturbances or blade vibrations. Using this approach, one first computes the time-mean (steady) flow about the airfoil by solving the steady flow equations using conventional computational fluid dynamic techniques. One then assumes that any unsteadiness in the flow is small and harmonic. The governing fluid equations of motion and the associated boundary conditions are then linearized about the mean flow solution to arrive at a set of linear variable coefficient equations that describe the small disturbance flow. The resulting linearized equations can be solved very efficiently. This technique was applied by Whitehead and Grant,[2] Verdon,[3] Hall and Crawley,[4] Holmes and Chuang,[5] Lindquist and Giles,[6] Cizmas and Hall,[7] and others to predict unsteady flows in turbomachinery cascades. Still, these linearized flow models predict the unsteady flow field for a single prescribed geometry and unsteady flow condition. These models give little or no information about the influence of design changes on steady and unsteady aerodynamic performance.

Only a few unsteady aerodynamic sensitivity analyses have been reported in the literature. We mention the previous work done by Murthy and Kaza[8] and by Lorence and Hall.[9,10] Murthy and Kaza[8] used a semianalytical panel method to describe the nominal flow. Lorence and Hall[9,10] modeled the flow through a two-dimensional cascade with the steady and linearized unsteady full potential equations, with rapid distortion theory used to model vortical flows. They used lower–upper (LU) decomposition to solve for the nominal steady and unsteady flow solutions. First, they solved the discretized steady flow equations using Newton iteration with LU decomposition. Then, they used one LU decomposition to solve the discretized small disturbance equations. They stored the LU decompositions from the nominal solution and used them to solve for the sensitivities of the steady and unsteady flow to changes in the design variables. Such an approach is extremely efficient for small systems where a matrix formulation of the nominal flow solver is available. For more complex flows modeled by the Euler equations, for example, the number of unknowns is relatively large. In such cases, a complete factorization of the global Jacobian of the nominal flow solver is too expensive. Instead, one may rely on incomplete factorization techniques and use the incompletely factored matrices as preconditioners in iterative solvers for multiple right-hand sides calculations. For details, we refer to a monograph by Saad.[11] Our experience has shown that for the practical case of computing aerodynamic sensitivities with respect to the airfoil shape, the direct approach based on incomplete factorization and iterative solvers is at least one or two orders of magnitude more expensive than one nominal solution.

In the past decade, a large amount of work has been done in the field of steady aerodynamic design and shape optimization, for example, by Pironneau,[12] Jameson,[13] Baysal and Eleshaky,[14] and

Presented as Paper 2000-0130 at the AIAA 38th Aerospace Sciences Meeting, Reno, NV, 10–13 January 2000; received 17 January 2000; revision received 12 November 2000; accepted for publication 22 November 2000.

*Assistant Research Professor, Department of Mechanical Engineering and Materials Science; currently Associate Research Engineer, United Technologies Research Center, East Hartford, CT 06040. Member AIAA.

†Associate Professor, Department of Mechanical Engineering and Materials Science. Associate Fellow AIAA.

Reuther and Jameson.[15] As suggested in Refs. 12 and 13, when the number of control parameters is relatively large (e.g., the number of parameters that define the airfoil shape), an adjoint method is more efficient. Two variations of the adjoint method are available, continuous and discrete adjoint methods. In the first case, the continuous adjoint equations, which are based on the linearization of the continuous governing equations, are formed and then discretized. Unfortunately, the computation of the sensitivities is affected by the truncation error of the discretization, which can be significant in the region of strong pressure gradients (e.g., at shock waves). Alternatively, in the discrete formulation, one forms a set of adjoint equations of the discretized flow equations. Such an approach gives the exact sensitivities of the numerical scheme. However, it may prove more difficult to implement because of the complexity of the numerical discretization. Also, depending on the implementation, the memory requirements may be much greater than that of the continuous adjoint method.

The goal of the present research is to develop adjoint equation methods for efficiently designing turbomachinery blading for improved aeroacoustic and aeroelastic performances. We consider two-dimensional cascade flows. Here we use a finite-volume two-step Lax–Wendroff discretization, as described by Hall[16] and Saxer.[17] Such a scheme is relatively simple to implement, easy to linearize, and has already been tested for linearized unsteady flow analyses.[18] To accelerate the convergence of the nominal solution, we use local time stepping and the multigrid accelerator described by Ni.[19] To improve the accuracy of the nominal flow solver, a continuously deforming grid is used. Once the nominal flow solution is obtained, the derivation of the discrete adjoint flow equations is straightforward. First, the linearization of the numerical discretization, without multigrid, is carried out. The adjoint flow equations are formed, and a multigrid procedure similar to the one developed for the nominal flow solver is implemented. Then, using the computed adjoint variables, the sensitivities of the user-defined objective functions with respect to each of the grid points on the airfoil are computed. Finally, using these sensitivities, we redesign the airfoils for improved performance.

In this paper, we apply the sensitivity analysis outlined above to redesign the shape of the airfoils of a cascade for increased aeroelastic stability. We also redesign the shape of the airfoils of an exit guide vane for reduced downstream radiated noise. The results obtained for two-dimensional turbomachinery flows indicate that the approach presented here is computationally efficient, yet still able to model the dominant flow physics. Ongoing research includes extending the discrete adjoint formulation method to more complex three-dimensional flows.

II. Nominal Flow Description

We start with the integral form of the Euler equations over a moving control volume $\hat{\Omega}$, that is,

$$\frac{\mathrm{d}}{\mathrm{d}t}\int_{\hat{\Omega}} \hat{\boldsymbol{q}}\,\mathrm{d}\hat{\Omega} + \oint_{\partial\hat{\Omega}} \left(\hat{\boldsymbol{F}}_T - \hat{\boldsymbol{q}}\frac{\partial \boldsymbol{f}^T}{\partial t}\right)\cdot \mathrm{d}\hat{\boldsymbol{S}} = \boldsymbol{0} \tag{1}$$

where $\boldsymbol{f}$ is the vector describing the position of the control volume $\partial\hat{\Omega}$, and $\mathrm{d}\hat{\boldsymbol{S}}$ is the elemental length of the boundary surface and points in the direction normal to the surface. The quantities $\hat{\boldsymbol{q}}$ and $\hat{\boldsymbol{F}}_T$ are the vector of conservation variables and the flux matrix, respectively, that is,

$$\hat{\boldsymbol{q}} = \begin{bmatrix} \hat{\rho} \\ \hat{\rho}\hat{u} \\ \hat{\rho}\hat{v} \\ \hat{\rho}\hat{e}_T \end{bmatrix}, \qquad \hat{\boldsymbol{F}}_T = [\hat{\boldsymbol{F}}, \hat{\boldsymbol{G}}] \tag{2}$$

where $\hat{\rho}$, $\hat{u}$, $\hat{v}$, and $\hat{e}_T$ are the static density, Cartesian components of velocity, and total specific energy.

We assume that the unsteadiness of the flow is small compared with the mean flow. The nonlinear unsteady flow is decomposed into a nonlinear mean (steady) flow and an unsteady small-disturbance flow. We also assume that the airfoils may exhibit a prescribed vibrational motion of known frequency ω. We use a strained coordinate system that moves with the airfoil near the airfoil, is stationary in the far field, and deforms smoothly inside the domain. The vector of conservation variables and the moving coordinates are assumed to exhibit a harmonic motion with frequency ω, so that

$$\begin{aligned} \hat{\boldsymbol{q}}(\xi,\eta,\tau) &= \boldsymbol{Q}(\xi,\eta) + \boldsymbol{q}(\xi,\eta)e^{j\omega\tau} \\ x(\xi,\eta,\tau) &= \xi + f(\xi,\eta)e^{j\omega\tau} \\ y(\xi,\eta,\tau) &= \eta + g(\xi,\eta)e^{j\omega\tau} \\ t(\xi,\eta,\tau) &= \tau \end{aligned} \tag{3}$$

where f and g are the Cartesian components of $\boldsymbol{f}$. Using Eq. (3), we then linearize the Euler equations, Eq. (1). After collecting zeroth and first-order terms, we obtain the mean flow Euler equations and the linearized unsteady Euler equations. For convenience, we write the resulting equations together,

$$\begin{aligned} &\oint_{\partial\Omega}\left(\begin{bmatrix} \boldsymbol{F}_T \\ \boldsymbol{F}'_T - j\omega\boldsymbol{Q}\boldsymbol{f}^T \end{bmatrix}\cdot \mathrm{d}\boldsymbol{S} + \begin{bmatrix} \boldsymbol{0} \\ \boldsymbol{F}_T \end{bmatrix}\cdot \mathrm{d}\boldsymbol{s}\right) \\ &\quad + \int_{\Omega} j\omega\left(\begin{bmatrix} \boldsymbol{0} \\ \boldsymbol{q} \end{bmatrix}\mathrm{d}\Omega + \begin{bmatrix} \boldsymbol{0} \\ \boldsymbol{Q} \end{bmatrix}\mathrm{d}\Omega'\right) = \boldsymbol{0} \end{aligned} \tag{4}$$

where

$$\boldsymbol{F}'_T = \left[\frac{\partial \boldsymbol{F}}{\partial \boldsymbol{Q}}\boldsymbol{q}, \frac{\partial \boldsymbol{G}}{\partial \boldsymbol{Q}}\boldsymbol{q}\right] \tag{5}$$

$$\mathrm{d}\Omega = \mathrm{d}\xi\,\mathrm{d}\eta, \qquad \mathrm{d}\Omega' = \mathrm{d}\xi\,\mathrm{d}g + \mathrm{d}x\,\mathrm{d}\eta$$

$$\mathrm{d}\boldsymbol{S} = \begin{bmatrix} \mathrm{d}\eta \\ -\mathrm{d}\xi \end{bmatrix}, \qquad \mathrm{d}\boldsymbol{s} = \begin{bmatrix} \mathrm{d}g \\ -\mathrm{d}f \end{bmatrix} \tag{6}$$

To complete the description of the unsteady flow problem, boundary conditions are specified on the airfoil surface and in the far field. In the far field, we use one-dimensional and two-dimensional Fourier nonreflecting boundary conditions as described by Hall and Crawley[4] and later by Giles.[20] Furthermore, we assume identical blades from passage to passage with spatially periodic blade motions. Then, for each interblade phase angle σ, the computational domain may be reduced to a single blade passage with additional periodic boundary conditions along the periodic boundaries.[21] Details of the boundary conditions derivations, their linearizations, and their implementations for the Euler equations are given in Ref. 18.

The resulting steady and unsteady equations, Eqs. (4–6), and associated appropriate boundary conditions can be treated as a single system of equations, with ω and σ as parameters. Any standard computational fluid dynamic (CFD) method may be used to discretize and integrate these equations. After discretization, a typical iterative method has the form

$$\delta\mathcal{Q}^k = \mathcal{Q}^{k+1} - \mathcal{Q}^k = \mathcal{N}(\mathcal{Q}^k;\alpha) \tag{7}$$

where

$$\mathcal{Q} = \begin{bmatrix} \boldsymbol{Q} \\ \boldsymbol{q} \end{bmatrix}, \qquad \mathcal{N}(\mathcal{Q};\alpha) = \begin{bmatrix} \boldsymbol{N}(\boldsymbol{Q};\alpha) \\ \boldsymbol{n}(\boldsymbol{Q},\boldsymbol{q};\alpha) \end{bmatrix} \tag{8}$$

The vector $\mathcal{Q}$ is the vector of steady and linearized unsteady conservation variables, k is the iteration number, and α the vector of user-defined designed variables, for example, thickness, camber, etc., or more generally, a discrete representation of the airfoil shape. The vector $\mathcal{N}$ is the vector of the discretized steady and linearized unsteady Euler equations and appropriate boundary conditions. Note that $\boldsymbol{N}(\boldsymbol{Q};\alpha)$ is a real nonlinear system of the discretized steady Euler equations and does not depend on $\boldsymbol{q}$. The vector $\boldsymbol{n}(\boldsymbol{Q},\boldsymbol{q};\alpha)$ is a complex linear system of the discretized unsteady Euler equations and has the same dimension as $\boldsymbol{N}(\boldsymbol{Q};\alpha)$. When converged, the nominal system of equations satisfies

$$\mathcal{N}(\mathcal{Q};\alpha) = 0 \tag{9}$$

III. Objective Functions

A. Aeroelastic Objective Functions

Once the nominal steady and unsteady flow solutions are known, we compute global aerodynamic characteristics such as the steady and unsteady lift and moment. We want to improve some of these aerodynamic characteristics by changing the airfoil geometry. Namely, we want to reduce unsteady aerodynamic loads due to gusts, increase aerodynamic damping, and decrease the coupled aeroelastic airfoil motion due to incoming gusts. In all these cases, we want the steady circumferential force acting of the airfoil to be constant, that is, any redesign of the airfoil should not change the turning.

First, we look separately at the unsteady aerodynamic response due to incoming gusts and airfoil motion. We denote by $J[\mathcal{Q}(\alpha), \alpha]$ the generic objective function we want to minimize. Specifically, we want to minimize the magnitude of the modal force (airfoil in plunge) due to an incoming unit gust:

$$J_{\text{gust}}[\mathcal{Q}(\alpha), \alpha] = |l_{\text{gust},h}| \tag{10}$$

Also, we want to increase the aerodynamic damping for a unit plunge, namely to decrease the imaginary part of the unsteady lift:

$$J_{\text{plunge}}[\mathcal{Q}(\alpha), \alpha] = \text{imag}(l_{\text{plunge},h})(< 0) \tag{11}$$

The quantities $l_{\text{gust},h}$ and $l_{\text{plunge},h}$ are the complex unsteady forces due to a unit gust and unit plunging in the direction of the blade plunging motion.

Next, we analyze the aeroelastic response of the blades to an incoming gust excitation. The airfoils are assumed to exhibit a harmonic plunging motion described by the aeroelastic equation

$$(-\Omega^2 + 1)\bar{h} = \left(4/\pi\mu\bar{\omega}_0^2\right)(l_{\text{gust},h} + \bar{h} l_{\text{plunge},h}) \tag{12}$$

where

$$\Omega = \omega/\omega_0, \qquad \bar{\omega}_0 = \omega_0 c/V_{-\infty}, \qquad \bar{h} = h/c$$
$$\mu = m/\pi\rho_{-\infty}(c/2)^2 \tag{13}$$

The quantity ω_0 is the first natural bending frequency of the blade, m is its mass, and h is the complex amplitude of the plunging motion. The derivation of this equation is described in Bisplinghoff et al.[22] For turbomachinery problems, the mass ratio, μ, is of order 100 or larger. The nondimensional complex plunging amplitude $\bar{h}$ described by Eq. (12) exhibits a peak at a reduced frequency $\bar{\omega}_P$:

$$\bar{\omega}_P = \bar{\omega}_0\sqrt{1 - \left[4/\left(\pi\mu\bar{\omega}_0^2\right)\right]\text{real}(l_{\text{plunge},h})} \tag{14}$$

which is very close to the reduced natural frequency of the elastic system. The value of the nondimensional amplitude is the absolute value of the $\bar{h}$, which, at $\bar{\omega} = \bar{\omega}_P$, reaches its peak value given by

$$|\bar{h}_P| = \left|\frac{l_{\text{gust},h}}{\text{imag}(l_{\text{plunge},h})}\right| \tag{15}$$

For this case, our goal is to minimize the amplitude peak of the aeroelastic blade motion $|\bar{h}_P|$, that is,

$$J_h[\mathcal{Q}(\alpha), \alpha] = \left|\frac{l_{\text{gust},h}}{\text{imag}(l_{\text{plunge},h})}\right| = \frac{J_{\text{gust}}}{-J_{\text{plunge}}} \tag{16}$$

while keeping the steady circumferential lift unchanged.

B. Aeroacoustic Objective Functions

In this section, we briefly analyze the aeroacoustic performance of a row of exit guide vanes (EGVs). We want to reduce the acoustic response of the EGV due to an incoming gust arising from the viscous wake of an upstream rotor. For more details about rotor–stator interactions, see Hall and Silkowski.[23] In the rotor frame of reference, steady viscous wakes are generated. A generic quantity $\hat{A}(x_R, y_R, t)$, which defines the wake, can be decomposed in a sum of stationary traveling waves, i.e.,

$$\hat{A} = \hat{A}(x_R, y_R, t) = \sum_n \tilde{A}(x_R)\exp[j(\omega_{R_n} t + \beta_{R_n} y_R)] \tag{17}$$

$$\omega_{R_n} = 0, \qquad \beta_{R_n} = 2\pi n/G_R, \qquad n = \pm 1, \pm 2, \ldots \tag{18}$$

The subscript R denotes the rotor frame of reference, G_R is the rotor blade-to-blade gap and β_{R_n} is the nth circumferential wave number. In the EGV frame of reference, the same wakes appear to be unsteady and the same quantity $\hat{A}$ is expressed as

$$\hat{A} = \hat{A}(x, y, t) = \sum_n \tilde{A}(x)\exp[j(\omega_n t + \beta_n y)] \tag{19}$$

Using the relationship between the two reference frames,

$$x_R = x, \qquad y_R = y - V_{\text{rotor}} t \tag{20}$$

the temporal frequency ω_n and the spatial wave number β_n in the EGV frame can be related to their counterparts in the rotor frame, that is,

$$\omega_n = -\beta_{R_n} V_{\text{rotor}} = \underbrace{(2\pi V_{\text{rotor}}/G_R)}_{\omega_{\text{BPF}}}(-n), \qquad \beta_n = \beta_{R_n} \tag{21}$$

The quantity ω_{BPF} is the blade passing frequency. Thus, the temporal frequency of any harmonics is just a multiple of the blade passing frequency. The corresponding interblade phase angle is given by

$$\sigma_n = \beta_n G = \beta_{R_n} G \tag{22}$$

where G is the stator blade-to-blade gap. Each frequency interblade phase angle pair (ω_n, σ_n) defines an incoming excitation for which we analyze the acoustic response of the stator.

Next, we reduce our analysis to one blade passage. We assume that the steady flow is uniform in the far field, both upstream and downstream. The response to any incoming perturbation is decomposed into a sum of incoming and outgoing traveling waves. For two-dimensional flows, the traveling waves are Fourier modes defined by their two spatial wave numbers. For each circumferential wave number, $\beta_{nm} = (\sigma_n + 2\pi m)/G$, or corresponding interblade phase angle, $\sigma_{nm} = \beta_{nm} G$, there are four axial wave numbers corresponding to two pressure modes (one incoming and one outgoing), one entropy mode, and one vorticity mode. The axial pressure wave numbers are given by

$$k_{nm_\pm} = \Big[-(\omega_n + \beta_{nm} V)U \pm \sqrt{(\omega_n + \beta_{nm} V)^2 - \beta_{nm}^2(U^2 - a^2)}\Big]\sqrt{(U^2 - 1)} \tag{23}$$

where U and V are the Cartesian components of the far-field flow velocity and a is the corresponding speed of sound. From Eq. (23) we see that depending on the far-field flow conditions and circumferential wave number β_{nm}, the axial wave number k_{nm} is either real or complex. If k_{nm} is complex, then this mode is cutoff, and the pressure mode decays exponentially away from the the cascade. However, when k_{nm} is real, the mode is cuton, and the outgoing pressure mode propagates with constant magnitude away from the cascade.

In this study, we identify the cuton modes, and then we attempt to minimize the participation of these modes in the acoustic response of the cascade by redesigning the airfoil shape. Specifically, the objective function is given by the magnitude of the propagating pressure mode, that is,

$$J_{\text{acoustic}}[\mathcal{Q}(\alpha), \alpha] = |p_{nm,\text{cuton}}| \tag{24}$$

IV. Sensitivity Analysis

A. Adjoint Flow Equations Description

First, we consider the unconstrained minimization problem. We want to minimize the objective function

$$I(\alpha) = J[\mathcal{Q}(\alpha), \alpha] \qquad \text{with} \qquad \mathcal{N}[\mathcal{Q}(\alpha), \alpha] = 0 \tag{25}$$

with no additional constraints. A typical optimization approach algorithm requires the computation of the gradient of the objective function $\nabla_\alpha I(\alpha)$.

To compute $\nabla_\alpha I(\alpha)$, it is convenient to define the Lagrangian associated with the constraint minimization problem, Eq. (25), that is,

$$\mathcal{L}(\mathcal{Q}, \alpha, \lambda) = J(\mathcal{Q}, \alpha) + \mathcal{N}^T(\mathcal{Q}, \alpha) \cdot \boldsymbol{\lambda} \tag{26}$$

where $\boldsymbol{\lambda}$ is a vector of as yet unknown Lagrange multipliers. Note that because $\mathcal{N}(\mathcal{Q}, \alpha)$ is zero, the Lagrangian has the same value as the cost function.

Next, we find the sensitivity of $\mathcal{L}$ to small changes in solution and geometry, $\delta\mathcal{Q}$ and $\delta\alpha$, that is,

$$\delta\mathcal{L} = \left(\nabla_\mathcal{Q} J + \nabla_\mathcal{Q}\mathcal{N}^T\lambda\right)^T \cdot \delta\mathcal{Q} + \left(\nabla_\alpha J + \nabla_\alpha\mathcal{N}^T\lambda\right)^T \cdot \delta\alpha \tag{27}$$

The evaluation of the partial derivatives appearing in Eq. (27) is a relatively easy and computationally inexpensive task. However, although $\delta\alpha$ is a prescribed quantity, $\delta\mathcal{Q}$ is not. Rather, $\delta\mathcal{Q}$ is a function of $\delta\alpha$ and is computationally expensive to evaluate. Thus, to eliminate the need to compute $\delta\mathcal{Q}$ in Eq. (27), we pick the vector of Lagrange multipliers $\boldsymbol{\lambda}$ so that first term vanishes, with the result that

$$\left[\nabla_\mathcal{Q}\mathcal{N}^T(\mathcal{Q}, \alpha)\right]\boldsymbol{\lambda} + \nabla_\mathcal{Q} J(\mathcal{Q}, \alpha) = 0 \tag{28}$$

Therefore,

$$\delta I(\alpha) = \underbrace{\left[\nabla_\alpha\mathcal{N}^T(\mathcal{Q}, \alpha) \cdot \boldsymbol{\lambda} + \nabla_\alpha J(\mathcal{Q}, \alpha)\right]^T}_{(\nabla_\alpha I)^T} \delta\alpha \tag{29}$$

In Eq. (28), the linear matrix operator $\nabla_\mathcal{Q}\mathcal{N}^T(\mathcal{Q}, \alpha)$ is the adjoint of the Jacobian of the nonlinear operator $\mathcal{N}(\mathcal{Q})$. This suggests that we can use similar solvers for both the nominal flow equation, Eq. (9), and the adjoint equation, Eq. (28), and expect similar convergence rates. In this analysis, we use a simple two-step Lax–Wendroff scheme with a multigrid accelerator, as described by Ni[19] and Hall.[16] Such a scheme has the advantage that is compact and relatively easy to linearize.

We first compute analytically the linearization of the Lax–Wendroff discretization, including the boundary conditions, but with no multigrid. This defines the basic adjoint iteration

$$\delta\boldsymbol{\lambda}^k = \boldsymbol{\lambda}^{k+1} - \boldsymbol{\lambda}^k = \left(\nabla_\mathcal{Q}\mathcal{N}^T\right)\boldsymbol{\lambda}^k + \nabla_\mathcal{Q} J \tag{30}$$

to which we apply a multigrid accelerator similar to the one used in the nominal scheme. Note that for two-dimensional problems, all the matrix and vector information necessary during iterations can be computed a priori and then stored in memory so that the iterative scheme for the adjoint problem reduces to only matrix vector multiplications. We found that the convergence histories for both the direct and the adjoint solver are similar, and one adjoint iteration (including multigrid sweeps) is about twice as expensive as the same iteration for the nominal solution.

B. Sensitivities and Airfoil Redesign

We now return to our original problem described in Sec. III. We seek to find

$$\min_\alpha I(\alpha) = \min_\alpha J[\mathcal{Q}(\alpha), \alpha] \qquad \text{with} \qquad \mathcal{N}(\mathcal{Q}; \alpha) = 0 \tag{31}$$

subject to the additional constraint that

$$I_0(\alpha) = J_0[\mathcal{Q}(\alpha), \alpha] = \text{const} \tag{32}$$

where, for example, $J_0[\mathcal{Q}(\alpha), \alpha]$ is the steady circumferential lift (steady aerodynamic force in the y direction). If we denote by $\mathcal{S}$ the search direction along which we minimize $I(\alpha)$ as described by Eqs. (31) and (32), then

$$\mathcal{S} = \boldsymbol{D}[\nabla_\alpha I(\boldsymbol{\alpha}) - \mu_\alpha \nabla_\alpha I_0(\boldsymbol{\alpha})] \tag{33}$$

where

$$\mu_\alpha = \frac{[\nabla_\alpha I(\boldsymbol{\alpha})]^T \cdot [\nabla_\alpha I_0(\boldsymbol{\alpha})]}{\left\|\nabla_\alpha I_0(\boldsymbol{\alpha})\right\|_2^2} \tag{34}$$

and $\boldsymbol{D}$ is the matrix of airfoil deformations, described in detail in an unpublished NASA report (K. C. Hall and R. Florea, "Sensitivity Analysis of Unsteady Inviscid Flow Through a Turbomachinery Cascade," 1999). Here, $\boldsymbol{\alpha}$ is a vector of normal displacements of all the points on the airfoil corresponding to grid node locations. If we allow arbitrary airfoil shapes, then the search direction (in the absence of constraints) would simply be the gradient of I with respect to $\boldsymbol{\alpha}$. However, to ensure smooth airfoil deformations, we instead define local smooth support functions (see below). Thus, not all airfoil shapes are permissible. The matrix $\boldsymbol{D}$ is a rank deficient square matrix that ensures the deformation of the airfoil is in the permissible design space defined by the support functions. With the addition of constraint functions, the search direction is also restricted to produce no change in the constraints. Note that the additional constraint given by Eq. (32) is satisfied to within a linear approximation.

To determine $\mathcal{S}$, we compute the sensitivities of two cost functions, $I(\boldsymbol{\alpha})$ and $I_0(\boldsymbol{\alpha})$, with respect to $\boldsymbol{\alpha}$. Note that in this paper I_0 is the steady lift, and only the solution of the real and much smaller adjoint steady equation needs to be computed. If no constraint is imposed, we simply take $\mu_\alpha = 0$.

There are different techniques to model the airfoil shape deformations. The main restriction here is that the new (redesigned), airfoil has a smooth surface. Although more sophisticated techniques are available, we use simple, smooth, local support sine-type deformations. For example on the upper surface of the airfoil, starting at the leading edge, the first normal deformation is defined by

$$T_1(s) = \sin^2(\pi s/\Delta s), \qquad 0 \le s \le \Delta s \tag{35}$$

where s is the coordinate arclength on the surface of the airfoil measured from the leading edge. The local support Δs is approximatively 40% of the upper-surface airfoil arclength. Then, this deformation is advanced over the airfoil surface with a constant step until it reaches the trailing edge. About 21 of these deformations are defined on each side of the airfoil.

We note that the grid points on the airfoil define all the possible airfoil shape deformations. In the present work, we first compute the sensitivities of the objective functions with respect to each grid point on the airfoil. Then, we use those local point sensitivities to compute the sensitivities of the actual shape deformations. Note that there is no need to regrid the flow domain or compute the sensitivities with respect to the interior grid deformations. Also, the sensitivity analysis is decoupled from the airfoil optimization process, and more sophisticated shape optimization techniques can be applied with minimum additional cost.

V. Results of Aeroelastic Sensitivity Analysis

The present adjoint formulation was applied to redesign the shape of the airfoils of a turbine blade for increased aeroelastic stability. We consider here the Fourth Standard Configuration, a typical turbine geometry that has been tested extensively by Bölcs and Fransson.[24] The stagger angle Θ is 56.6 deg, and the gap-to-chord ratio G is 0.76. The inflow Mach number $M_{-\infty}$ is 0.26, and the inflow angle $\Omega_{-\infty}$ (measured from the axial direction) is 50 deg. The flow is completely subsonic, with a Mach number downstream M_∞ of approximately 0.79.

A. Nominal Flow Equations Solution

The computational domain is defined by a single blade passage and is discretized using an H-type grid. Three computational grids are used in the present study: a coarse node grid (65 nodes in the streamwise direction and 17 nodes in the cross-flow direction), a medium grid (129×33 nodes) shown in Fig. 1, and a fine grid

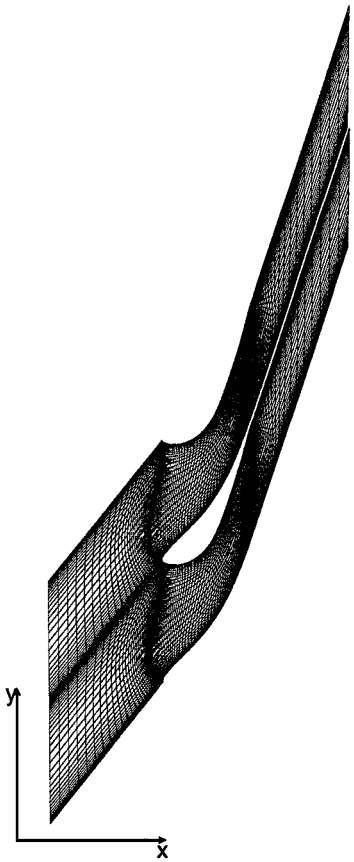

Fig. 1 129 × 33 node H grid.

(257 × 49 nodes). Multiple passages are shown for clarity in Fig. 1. For each of these grids, we first compute the steady (mean) flow field solution. Once the mean flow field solution is determined, we compute the unsteady flow due to two different types of external excitations. Namely, we compute the unsteady flow due to an incoming vortical gust and the unsteady flow due to plunging motion of the airfoils. The plunging direction makes a 60.4 deg angle with the airfoil chord. The unsteady calculations correspond to an interblade phase angle $\sigma = -90$ deg and a reduced frequency $\bar{\omega} = \omega c / V_{-\infty} = 1.0$, where $V_{-\infty}$ is the inlet velocity and c is the blade chord.

Shown in Figs. 2 and 3 are the steady and unsteady pressure distributions for the three different grid resolutions. In Fig. 2, we have shown the steady pressure distribution and the real and imaginary unsteady pressure due to an incoming vortical gust. In Fig. 3, we show the real and imaginary unsteady pressure due to plunging motion. In all cases, note the good agreement between the coarse, medium, and fine grid solutions. For all practical purposes, the medium grid solutions are grid converged; thus, the medium. resolution grid will be used for calculations in the following, unless otherwise indicated.

B. Adjoint Flow Equations Solution

Next we evaluate the sensitivities of the objective functions described by Eqs. (10), (11), and (16) for the steady and unsteady flow solutions computed in Sec. V.A.

Following Eqs. (29), (33), and (34), we first compute the adjoint flow equations solutions for two different objective functions: the magnitude of the modal force (airfoil in plunge) due to an incoming unit gust [see Eq. (10)] and the aerodynamic damping due to a unit plunge [see Eq. (11)]. We also compute the adjoint flow equations solution for the steady constraint $J_0[\mathcal{Q}(\alpha), \alpha]$, the steady circumferential lift. We show in Fig. 4 the convergence history for the adjoint solver with and without multigrid on the medium grid. For comparison, we also show the convergence histories for the direct flow solver. The unsteady flow conditions correspond an incoming gust with $\sigma = -90$ deg, $\bar{\omega} = 1$. The results show that the direct and adjoint iterations have the same terminal convergence rate and, furthermore, that the multigrid accelerator is extremely effective.

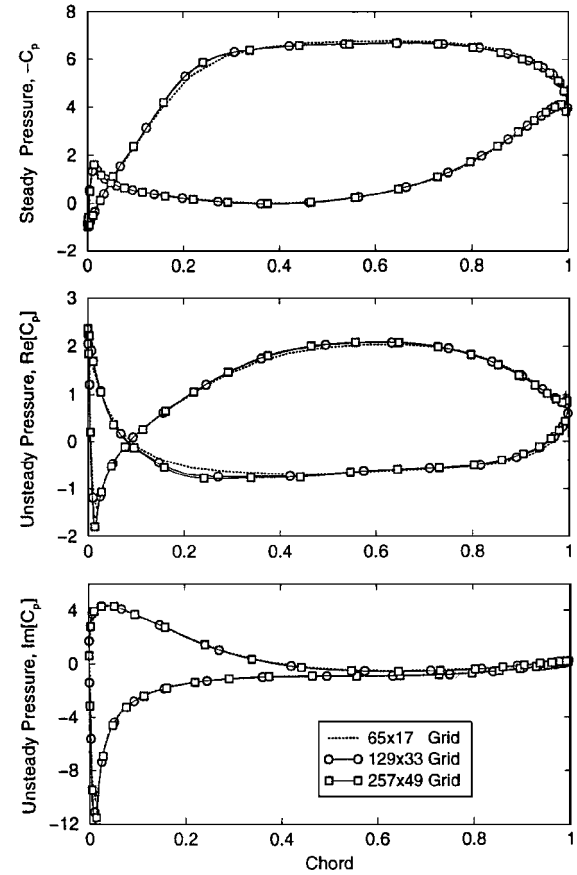

Fig. 2 Steady pressure distribution and real and imaginary unsteady pressure due to incoming gust. Steady flow conditions: $M_{-\infty} = 0.26$, $\Omega_{-\infty} = 50$ deg. Unsteady flow conditions: $\sigma = -90$ deg, $\bar{\omega} = 1$.

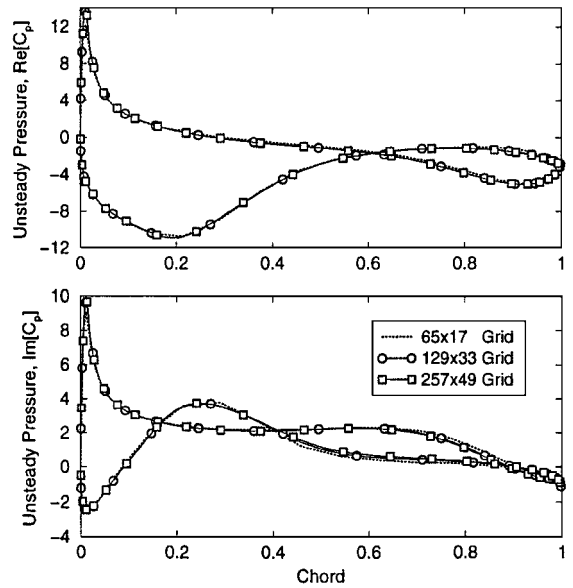

Fig. 3 Real and imaginary unsteady pressure due to plunging motion. Steady flow conditions: $M_{-\infty} = 0.26, \Omega_{-\infty} = 50$ deg. Unsteady flow conditions: $\sigma = -90$ deg, $\bar{\omega} = 1$.

In Figs. 5 and 6, we show the sensitivity of the unsteady lift with respect to the local normal deformations of the airfoil for the three different grid resolutions. In the case of unsteady flow due to an incoming gust, the sensitivities computed on the three different grids are in excellent agreement with one another. This suggests that we can use the coarse grid solution to find the gradient of the cost function and then use this gradient as a search direction on a finer grid. Also, for some points on the airfoil, a finite difference approach

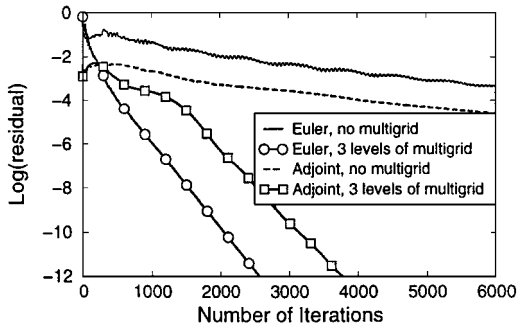

Fig. 4 History convergence of nominal and adjoint steady and unsteady flow equation solvers: 129 × 33 node H grid.

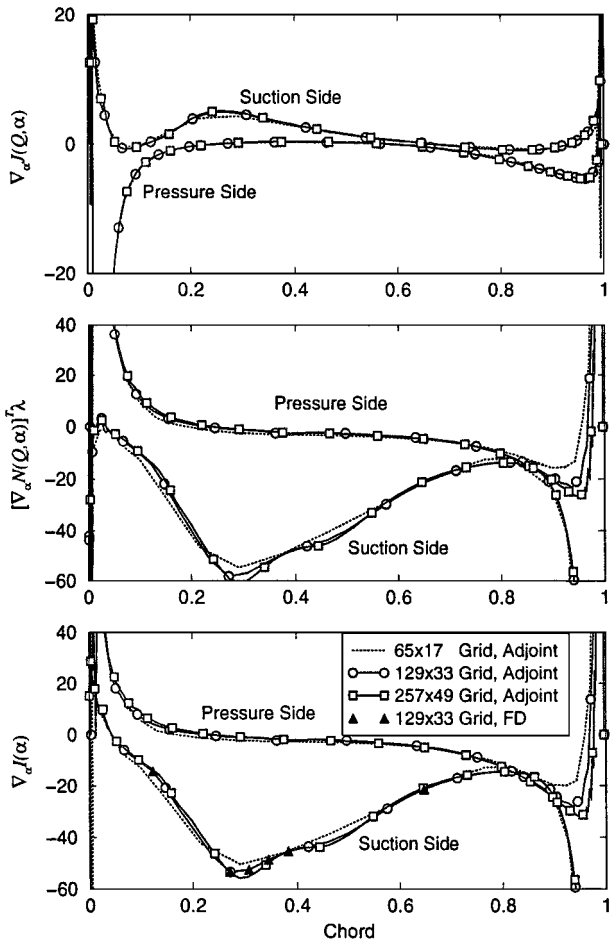

Fig. 5 Sensitivities of the unsteady lift amplitude due to incoming gust with respect to local normal deformations: $I(\alpha) = |l_{\text{gust},h}|$.

was used to numerically compute the sensitivities to local normal deformations. The results obtained show very good agreement with the present approach based on an adjoint variable formulation. In the case of airfoil plunging motion, the local normal sensitivities show a somewhat slower grid convergence, but the results are still quite acceptable.

C. Airfoil Shape Optimization

Next, using the sensitivities presented in Figs. 5 and 6, we redesigned the Fourth Standard Configuration airfoils for the objective function defined by Eq. (16) and with the steady flow constraint.

We note that the (inviscid) sensitivities shown in Figs. 5 and 6 are quite large near the leading and trailing edges of the airfoil, suggesting that large changes in the objective function can be achieved for modest changes in the airfoil shape. However, as a practical matter, local shapes changes in these regions cannot be accurately analyzed without a more detailed viscous analysis. Thus, so as not to produce

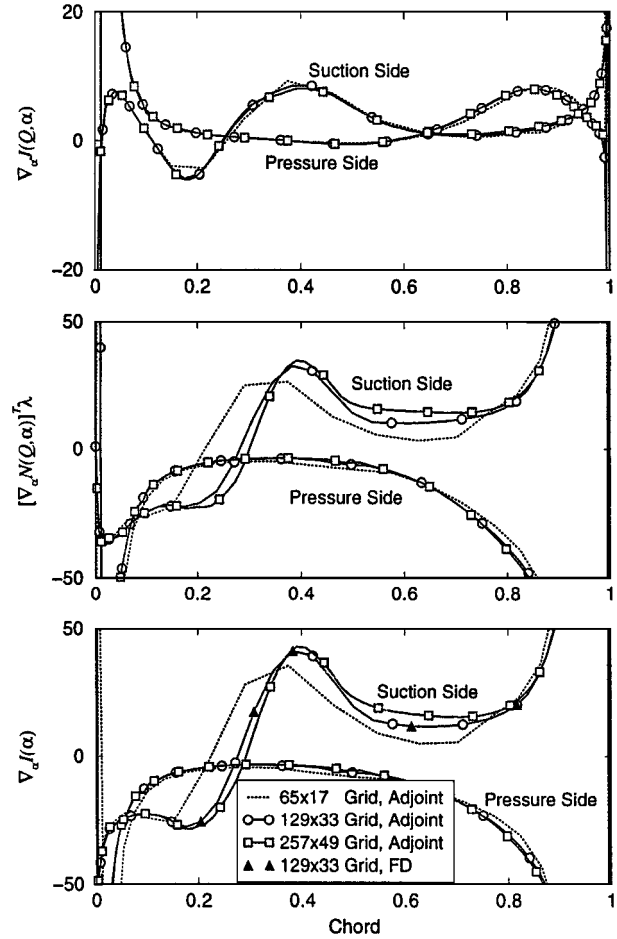

Fig. 6 Sensitivities of the imaginary part of the unsteady lift due to airfoil plunging with respect to local normal deformations: $I(\alpha) = \text{imag}(l_{\text{plunge},h})$.

nonphysical sensitivities, we define our particular airfoil deformations as described in Sec. IV.B, limiting the amount of shape change allowed at the leading and trailing edges.

We show in Figs. 7 and 8 the results obtained for the minimization of the maximum nondimensional amplitude of the plunging motion $|\bar{h}_P|$ arising from an incident gust, defined by Eq. (16), with the steady lift constraint imposed. As we can see from Eq. (16), this corresponds to both decreasing the unsteady lift due to the incoming gust, $|l_{\text{gust},h}|$, and increasing the aerodynamic damping, $-\text{imag}(l_{\text{plunge},h})$. Shown in Fig. 7 are, from top to bottom, the steady pressure distribution, the components of the unsteady pressure distribution due to plunging, the airfoil shapes, and the variation of the steady and unsteady objective functions. We define the deformation area to be the absolute value of the area enclosed between the modified and nominal airfoil surfaces. We note that the steady lift constraint and the steady pressure distribution proved to be extremely restrictive. To maintain a reasonably small adverse steady pressure gradient, a decrease of only 8% of $|l_{\text{gust},h}|$ can be obtained. The variation in aerodynamic damping is much larger, at least 35%, for reasonably small adverse steady pressure gradients. The corresponding variation in $|\bar{h}_P|$ is around 33%. The small steady lift variation, about 0.3%, is due to the fact that the steady lift constraint, Eq. (32), is satisfied only within a linear approximation.

VI. Results of Aeroacoustic Sensitivity Analysis

The present adjoint formulation was also applied to reduce downstream radiated noise from a cascade of EGVs, typical for modern high-bypass ratio fans. The nominal airfoil shape is a slightly modified NACA 8508-65 profile. The ratio of the number of fan rotor blades to exit guide vanes, N_R/N_{EGV}, is 0.4. The blade-to-blade gap G is 1.0, the inlet Mach number $M_{-\infty}$ is 0.5, the inlet flow angle $\Omega_{-\infty}$ is 30 deg, and the stagger angle Θ is 16 deg. The wheel speed

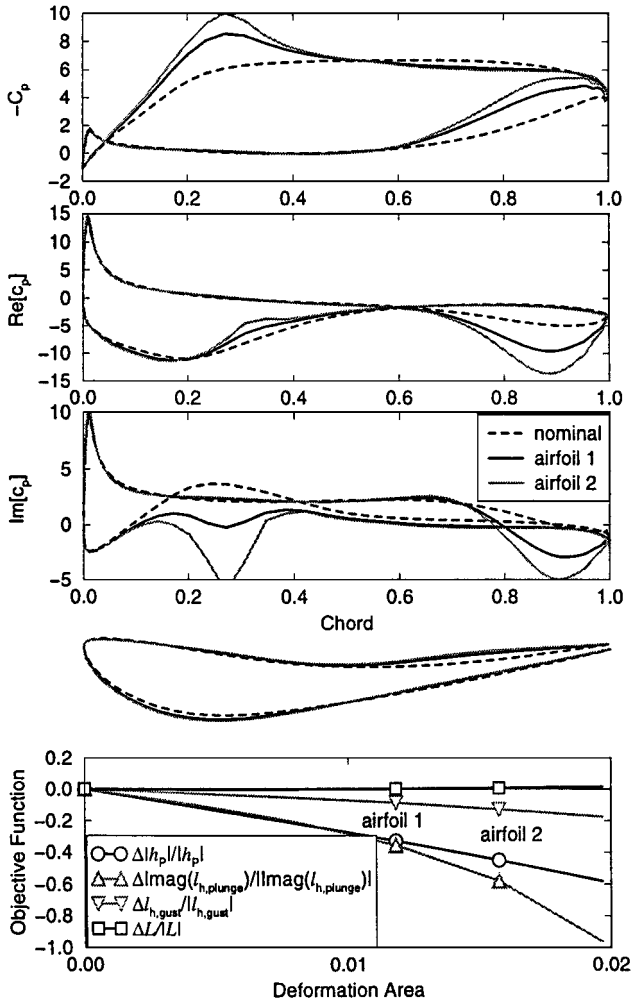

Fig. 7 Steady and unsteady pressure distributions for different airfoil shapes. Unsteady flow due to airfoil plunging motion induced by gust excitation. Minimize $|\bar{h}_P|$ given by Eq. (15), with steady lift constraint. Component of the unsteady pressure distribution due to plunging.

of the upstream rotor V_{rotor} is $1.5 \times V_{-\infty}$, where $V_{-\infty}$ is the inlet velocity in the absolute frame. The same configuration was analyzed previously by Lorence and Hall.[10]

A. Nominal Flow Equations Solution

As before, the computational domain is defined by a single blade passage and is discretized using a 129×49 node H grid shown in Fig. 9. First we compute the steady flow solution. The computed exit Mach number M_∞ is 0.413, and the exit flow angle Ω_∞ is 4.7 deg. Based on these values, a modal (Fourier) analysis indicates that the acoustic response of this cascade to excitations at the first passing frequency $\bar{\omega}_{n=-1} = \bar{\omega}_{\text{BPF}} = 3.77$ is cutoff. For incoming gust excitations at twice the blade passing frequency, $\bar{\omega}_{n=-2} = 2\bar{\omega}_{\text{BPF}} = 7.54$, a pressure mode with $\sigma_{n=-2,m=1} = 72$ deg is cuton in both the upstream and downstream region (Table 1).

We analyzed the acoustic response of the stator to a vortical incoming gust with unit amplitude at a reduced frequency $\bar{\omega} = 2\bar{\omega}_{\text{BPF}} = 7.54$ and interblade phase angle $\sigma = -288$ deg. A unit amplitude gust is one in which the magnitude of the perturbation velocity normal to the steady flow direction (down-wash) would be unity at the leading edge of the airfoil if the steady flow were uniform and undeflected by the EGV. The real and imaginary parts of the unsteady surface pressure computed using the present analysis are shown in Fig. 10. Also shown for comparison is the pressure distribution computed using the linearized potential rapid distortion theory (RDT) analysis of Lorence and Hall.[10] A relatively good agreement between the two sets of results is observed.

Table 1 Two-dimensional Fourier analysis of the far-field unsteady flow for EGV cascade

n	σ_{R_n}, deg	$\bar{\omega}_n$	m	σ_{nm}, deg	Cuton
−1	−144.0	3.7699	−2	−864.0	
			−1	−504.0	
			0	−144.0	
			1	216.0	
			2	576.0	
1	144.0	−3.7699	−2	−576.0	
			−1	−216.0	
			0	144.0	
			1	−504.0	
			2	−864.0	
−2	−288.0	7.5398	−2	−1008.0	
			−1	−648.0	
			0	−288.0	
			1	72.0	yes
			2	432.0	
2	288.0	−7.5398	−2	−432.0	
			−1	−72.0	yes
			0	288.0	
			1	648.0	
			2	1008.0	

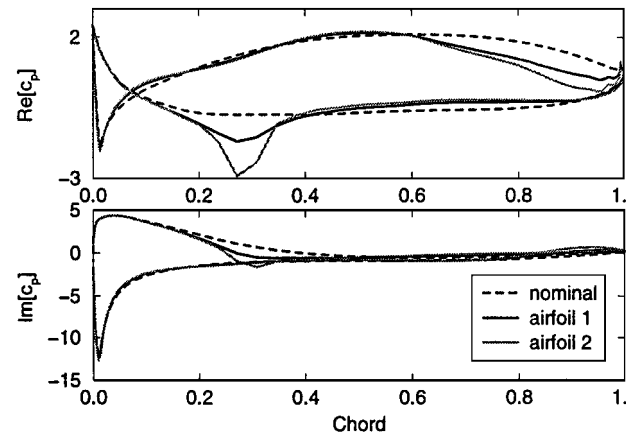

Fig. 8 Steady and unsteady pressure distributions for different airfoil shapes. Unsteady flow due to airfoil plunging motion induced by gust excitation. Minimize $|\bar{h}_P|$ given by Eq. (15), with steady lift constraint. Component of the unsteady pressure distribution due to incoming gust.

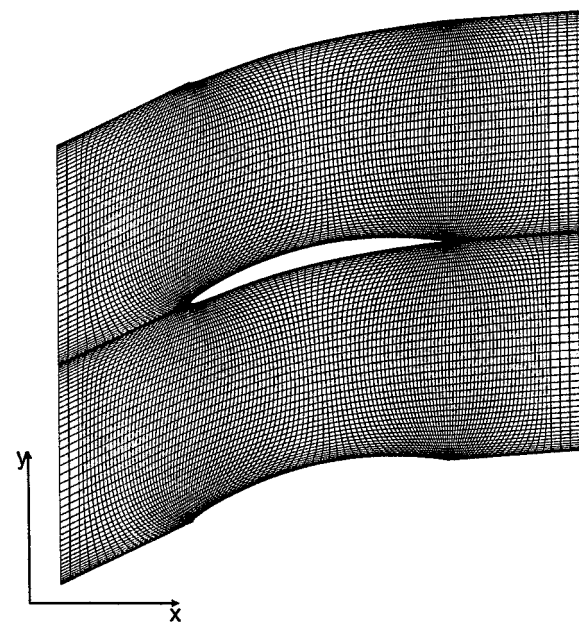

Fig. 9 129 × 49 node H grid for a cascade of EGVs.

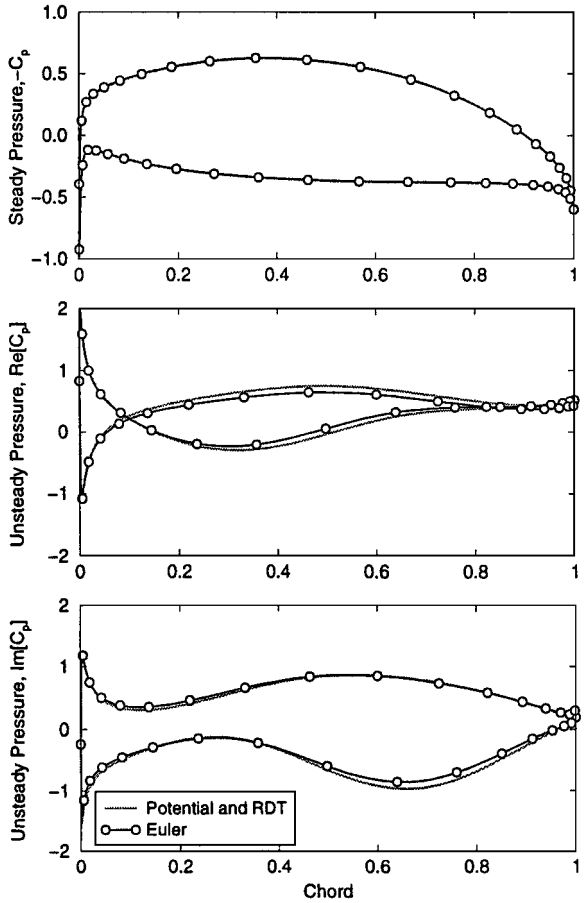

Fig. 10 Steady and unsteady pressure distribution on EGV airfoils. From top to bottom: steady pressure distribution, real and imaginary unsteady pressure due to incoming gust. Steady flow conditions: $M_{-\infty} = 0.5$, $\bar{\Omega}_{-\infty} = 30$ deg. Unsteady flow conditions: $\sigma = -288$ deg, $\bar{\omega} = 7.54$.

B. Adjoint Flow Equations Solution

Next we computed the sensitivities of the objective function defined by the acoustic response of the cascade, Eq. (24), for the unsteady solution presented in the previous section. The aeroacoustic objective function depends directly on the pressure in the far field and only indirectly on the airfoil shape. Hence, the last term in the right-hand side of Eq. (29) is zero. Shown in Fig. 11 are sensitivities of the cuton unsteady downstream-outgoing pressure mode with respect to local normal deformations of the airfoil surface. The objective function for this case is the propagating pressure mode, $I(\alpha) = |p_{nm,\ \mathrm{cuton}}|$, with $n = -2$, $m = 1$. We note that the maximum variation in the sensitivity is obtained for local normal deformations at the leading and trailing edge. However, when combined into local support sine-type smooth deformations, the effect of these two regions is dramatically reduced.

C. Airfoil Shape Optimization

Next we used the sensitivities presented in Fig. 11 to redesign the EGVs for lower downstream acoustic radiation with and without the steady lift constraint. We used simple local support sine-type deformations that proved to be more effective in reducing the objective function, while preserving the original smoothness of the airfoil shape. We show in Figs. 12 and 13 the results obtained for the minimization of the cuton unsteady downstream-outgoing pressure mode due to an incoming vortical gust using the local support deformations. The steady and unsteady pressure distributions shown in Fig. 12 are unconstrained sensitivities, whereas in Fig. 13 the additional steady lift constraint is imposed. As before, we show the steady, real unsteady, and imaginary unsteady pressure distributions, the airfoil shapes, and the objective function variations. The magnitude of the downstream unsteady pressure wave was reduced about 18% for the unconstrained case and about 17.5% for

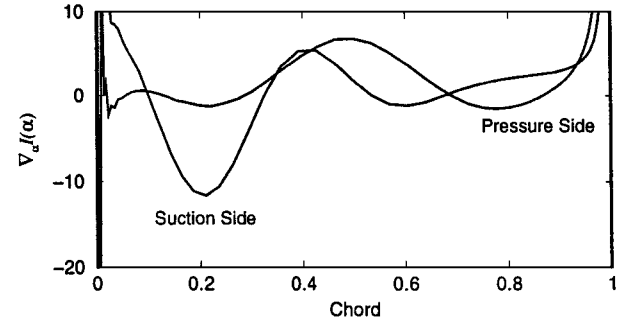

Fig. 11 Sensitivities of the cuton unsteady downstream-outgoing pressure Fourier mode with respect to local normal deformations: $I(\alpha) = |p_{nm,\ \mathrm{cuton}}|$, $n = -2$, $m = 1$.

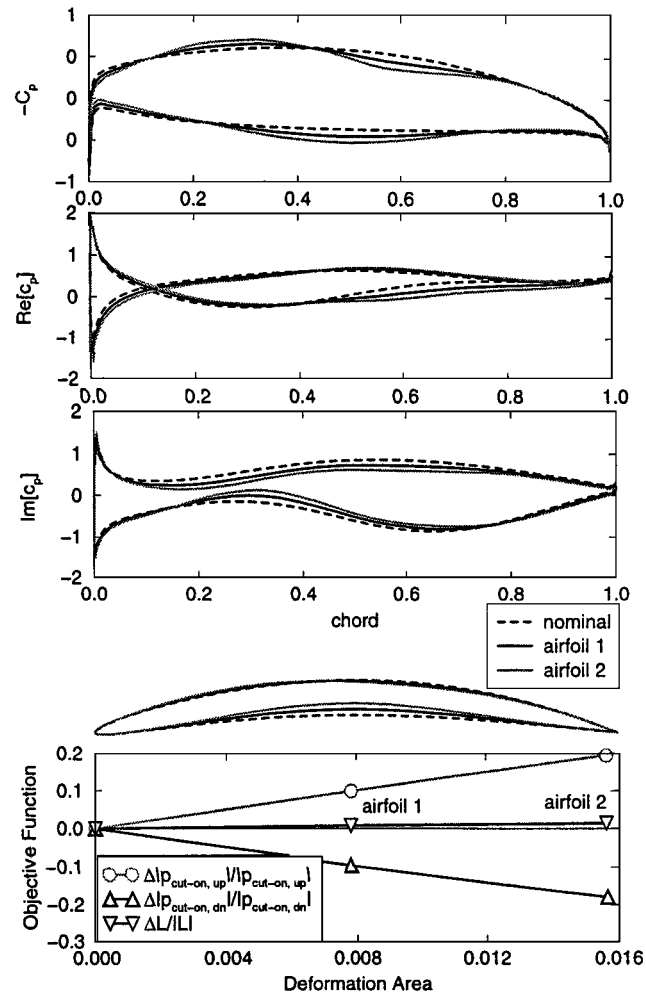

Fig. 12 Steady and unsteady pressure distributions for different airfoil shapes. Unsteady flow due to incoming gust. Minimize the cuton unsteady downstream-outgoing pressure Fourier mode, $|p_{\mathrm{cuton,\ dn}}|$, given by Eq. (24), with no steady lift constraint. $|p_{\mathrm{cuton,\ up}}|$ is the cuton unsteady upstream-outgoing pressure Fourier mode.

the constrained steady lift case, from 0.242 to about 0.198 and 0.200 respectively. These variations correspond to about 1.7 dB reduction in sound pressure level (SPL). Upstream, the magnitude of the unsteady upstream-outgoing pressure mode was increased by 20% in both cases, from 0.101 to about 0.121.

We note that the steady lift constraint proved to have little effect in this case. As a practical matter, the main restriction on the design is to maintain a reasonable thickness of the airfoil. We also want adverse pressure gradients that are small enough that the flow does not separate.

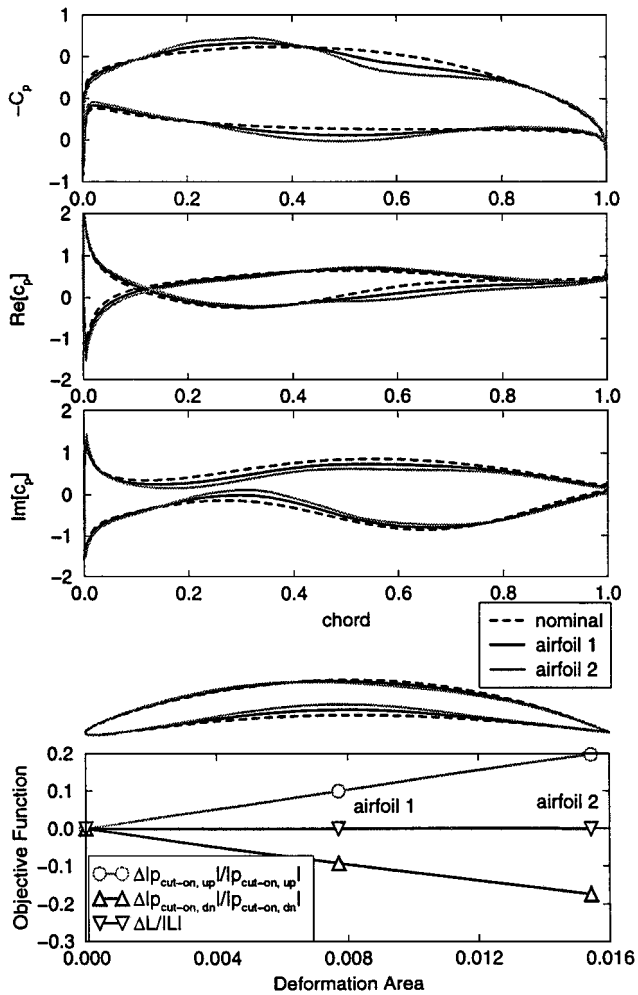

Fig. 13 Steady and unsteady pressure distributions for different airfoil shapes. Unsteady flow due to incoming gust. Minimize the cuton unsteady downstream-outgoing pressure Fourier mode, $|p_{\text{cuton, dn}}|$, given by Eq. (24), with steady lift constraint. $|p_{\text{cuton, up}}|$ is the cuton unsteady upstream-outgoing pressure Fourier mode.

By way of comparison, the use of design variables such as thickness, camber, and reflex may not allow enough flexibility in the design to produce a large reduction in the objective function. As an example, using only these global airfoil definitions as basis for the global deformations, only a 6% downstream pressure wave reduction was obtained. Similar results were reported in Ref. 10.

VII. Conclusions

In this paper, we present a novel approach for computing the sensitivity of two-dimensional unsteady inviscid aerodynamic flow through turbomachinery cascades to changes in geometry. We model the flow with the steady and linearized unsteady Euler equations, which are discretized using a finite-volume two-step Lax–Wendroff discretization with local time stepping and a multigrid accelerator. We first compute the nominal steady and linearized unsteady flow field solutions, computing the unsteady aerodynamic forces due to an incoming gust and plunging motion of the cascade airfoils. We also compute the aeroacoustic response to incoming gusts. Next the basic CFD scheme and the corresponding boundary conditions are linearized, and the adjoint of the discretized system of equations is formed. A multigrid technique is used to accelerate the convergence of the adjoint flow equation solver. For each objective function, the adjoint flow equation solutions are computed. Similar convergence rates are obtained for both the nominal and the adjoint solver. The computed adjoint variables are used to compute efficiently the sensitivities of the aeroelastic and aeroacoustic objective functions with respect to airfoil geometry. To model the airfoil shape deformations, we use simple, smooth, local support deformations.

We applied the sensitivity analysis to redesign the Fourth Standard Configuration turbine geometry for improved aeromechanical performances. For this configuration we obtained an 8% reduction in the unsteady lift due to an incoming gust. Maintaining the steady lift and a reasonably small adverse pressure gradient proved to be extremely restrictive constraints. However, under similar restrictions, we were able to also increase the aerodynamic damping, thereby decreasing the aeroelastic airfoil motion by at least 33%.

We also applied the sensitivity analysis to reduce the downstream radiated noise from a cascade of EGVs. A 1.7-dB reduction in the downstream sound pressure level magnitude was obtained. In this case, the main restriction proved to be the thickness of the airfoil. Also, an undesired increase in the upstream sound pressure level accompanied the decrease in the aft sound pressure level. This behavior was previously observed by Lorence and Hall,[10] and suggests that the changes in the airfoil shape produce destructive interferences downstream but constructive interferences upstream.

The present method is quite general and is easily extended to more complex viscous or three-dimensional flows; work is currently underway to extend the method to three-dimensional flows.

References

[1]Gliebe, P. R., "Aeroacoustics in Turbomachines and Propellers—Future Research Needs," *Unsteady Aerodynamics, Aeroacoustics, and Aeroelasticity of Turbomachines and Propellers*, edited by H. M. Atassi, Springer-Verlag, New York, 1993, pp. 619–642.

[2]Whitehead, D. S., and Grant, R. J., "Force and Moment Coefficients of High Deflection Cascades," *Proceedings of the 2nd International Symposium on Aeroelasticity in Turbomachines*, edited by P. Suter, Juris-Verlag, Zurich, 1981, pp. 85–127.

[3]Verdon, J. M., "Linearized Unsteady Aerodynamic Theory," *Manual on Aeroelasticity in Axial-Flow Turbomachines, Unsteady Turbomachinery Aerodynamics*, edited by M. F. Platzer and F. O. Carta, Vol. 1, AG-298, AGARD, 1981, Chap. 2.

[4]Hall, K. C., and Crawley, E. F., "Calculation of Unsteady Flows in Turbomachinery Using the Linearized Euler Equations," *AIAA Journal*, Vol. 27, No. 6, 1989, pp. 777–787.

[5]Holmes, D. G., and Chuang, H. A., "2D Linearized Harmonic Euler Flow Analysis for Flutter and Forced Response," *Unsteady Aerodynamics, Aeroacoustics, and Aeroelasticity of Turbomachines and Propellers*, edited by H. Atassi, Springer-Verlag, New York, 1993, pp. 213–230.

[6]Lindquist, D. R., and Giles, M. B., "On the Validity of Linearized Euler Equations with Shock Capturing," *AIAA Journal*, Vol. 32, No. 1, 1994, pp. 46–53.

[7]Cizmas, P. G. A., and Hall, K. C., "Computation of Steady and Unsteady Viscous Flows Using a Simultaneously Coupled Inviscid-Viscous Interaction Technique," *Journal of Fluids and Structure*, Vol. 9, Aug. 1995, pp. 639–657.

[8]Murthy, D., and Kaza, K., "Semianalytical Technique for Sensitivity Analysis of Unsteady Aerodynamic Computations," *Journal of Aircraft*, Vol. 28, No. 8, 1991, pp. 481–488.

[9]Lorence, C. B., and Hall, K. C., "Sensitivity Analysis of Unsteady Aerodynamics Loads in Cascades," *AIAA Journal*, Vol. 33, No. 9, 1995, pp. 1604–1610.

[10]Lorence, C. B., and Hall, K. C., "Sensitivity Analysis of the Aeroacoustic Response of Turbomachinery Blade Rows," *AIAA Journal*, Vol. 34, No. 9, 1996, pp. 1545–1554.

[11]Saad, Y., *Iterative Methods for Large Linear Systems*, PWS Publishing, Boston, 1996.

[12]Pironneau, O., *Optimal Shape Design for Elliptic Systems*, Springer-Verlag, New York, 1984.

[13]Jameson, A., "Aerodynamic Design via Control Theory," *Journal of Scientific Computing*, Vol. 3, No. 3, 1988, pp. 233–260.

[14]Baysal, M., and Eleshaky, O., "Aerodynamic Sensitivity Analysis Methods for the Compressible Euler Equations," *Journal of Fluids Engineering*, Vol. 113, No. 4, 1991, pp. 681–688.

[15]Reuther, J., and Jameson, A., "Aerodynamic Shape Optimization of Wing and Wing-Body Configurations Using Control Theory," AIAA Paper 95-0123, Jan. 1995.

[16]Hall, M. G., "Cell-Vertex Multigrid Solutions Schemes for Solutions of the Euler Equations," *Proceedings of the IMA Conference on Numerical Methods in Fluids, Oxford 1985*, edited by M. B. K.W. Morton, Oxford Univ. Press, Oxford, 1986.

[17]Saxer, A. P., "A Numerical Analysis of 3-D Inviscid Stator/Rotor Interactions Using Non-Reflecting Boundary Conditions," Gas Turbine Lab. Rept. 209, Massachusetts Inst. of Technology, Cambridge, MA, March 1992.

[18]Hall, K. C., and Clark, W. S., "Linearized Euler Prediction of Unsteady

Aerodynamic Loads in Cascades," *AIAA Journal*, Vol. 31, No. 3, 1993, pp. 540–550.

[19]Ni, R., "A Multiple Grid Scheme for Solving the Euler Equations," *AIAA Journal*, Vol. 20, No. 11, 1982, pp. 1565–1571.

[20]Giles, M. B., "Non-Reflecting Boundary Conditions," *AIAA Journal*, Vol. 28, No. 12, 1990, pp. 2050–2058.

[21]Whitehead, D. S., "Force and Moment for Vibratory Aerofoils in Cascades," British Aeronautical Research Council, R and M 3254, London, 1960.

[22]Bisplinghoff, R. L., Ashley, H., and Halfman, R. L., *Aeroelasticity*, Addison–Wesley, Cambridge, 1955.

[23]Hall, K. C., and Silkowski, P. D., "The Influence of Neighboring Blade Rows on the Unsteady Aerodynamic Response of Cascades," *Journal of Turbomachinery*, Vol. 119, No. 1, 1997, pp. 85–93.

[24]Bölcs, A., and Fransson, T. H., "Aeroelasticity in Turbomachines. Comparison of Theoretical and Experimental Results," U.S. Air Force Office of Scientific Research, AFOSR-TR-87-0605, Washington, DC, 1986.

P. J. Morris
Associate Editor